ISSN 1330-3651
UDC/UDK 681.523.5:004.896

DYNAMIC MODELING OF ONE DEGREE OF FREEDOM PNEUMATIC MUSCLE-BASED ACTUATOR FOR INDUSTRIAL APPLICATIONS

Alexander Hošovský, Michal Havran

Preliminary notes

Pneumatic artificial muscles belong to the group of nonconventional actuators intended for various biomedical or industrial applications. The one-DOF actuator (DOF – degree of freedom) consists of two muscles acting in opposition to each other (antagonistic connection) with simplified control scheme (stiffness control loop is excluded in order to simplify the control and to achieve as high stiffness as possible). The actuator exhibits nonlinear behaviour attributable to the compliant nature of pneumatic muscles. The muscle model is based on modified two-element muscle model consisting of a variable damper and a variable spring connected in parallel. From kinematic point of view, it is a simple mechanism with one degree of freedom (arm with added mass rotating around one revolute axis) with plane of movement being parallel to the ground. The main purpose of this model is a control design, so the stringency of accuracy criteria is lowered compared to a truth model. The model is validated using the results of dynamic experiments with real plant in laboratory conditions.

Keywords: *actuator, dynamic response, force, pneumatic artificial muscle, spring*

Dinamičko modeliranje aktuatora na bazi pneumatskog mišića s jednim stupnjem slobode za industrijsku primjenu

Prethodno priopćenje

Pneumatski umjetni mišići spadaju u skupinu nekonvencionalnog aktuatora za različitu biomedicinsku ili industrijsku primjenu. Jedan DOF aktuator sastoji se od dva mišića koji djeluju suprotno jedan od drugog (antagonistička veza) s pojednostavnjenom regulacijskom shemom (regulacijska petlja stabilnosti je isključena kako bi se pojednostavila regulacija i kako bi se postigla što viša stabilnost). Aktuator pokazuje nelinearno ponašanje sukladno prirodi pneumatskih mišića. Model mišića temelji se na modificiranom modelu mišića s dva elementa koji se sastoji od varijable amortizera i varijable opruge spojenih paralelno. Iz kinematičke točke gledišta, to je jednostavan mehanizam s jednim stupnjem slobode (ruka s dodanom masom koja rotira oko jedne okretne osi) s ravninom gibanja paralelnom s tlom. Glavna svrha ovog modela je kontrola konstrukcije, tako da je strogost kriterija točnosti smanjena u odnosu na stvarni model. Model je potvrđen uporabom rezultata dinamičkih pokusa sa stvarnom opremom u laboratorijskim uvjetima.

Ključne riječi: *aktuator, dinamički odziv, sila, pneumatski umjetni mišić, opruga*

1 Introduction

Pneumatic artificial muscles are nonconventional pneumatic actuators with certain properties comparable to human skeletal muscles. Basically they consist of a rubber tube with nonextensible braiding made of various materials (e.g. nylon). Their light construction and high values of generated forces combined with the capability of working in dangerous environments make them attractive for certain applications in biomedical or industrial area. The positive characteristics of this actuator are somewhat impaired by the nonlinearities inherently associated with its compliant character. This makes the process of modelling more difficult and limits the possibilities for applying linear control techniques.

The design of control systems usually assumes the availability of a plant model, which simulates the behaviour of a plant under various operating conditions [1]. Even though there are techniques which allow a model-free control design (e.g. fuzzy logic), it is still advantageous to have a mathematical model of relevant plant (in this case it can be used for offline optimization of fuzzy control system for instance) [2÷8]. The modelling of pneumatic artificial muscles and systems based on them was the subject of a number of works. One of the pioneering works was [9] where a thorough static and dynamic testing was carried out for McKibben pneumatic artificial muscles together with the comparison of obtained results to their biological counterparts. In [10] more detailed modelling of braid effects on contractile range and friction was introduced and these modifications were incorporated into enhanced static and dynamic model of a pneumatic artificial muscle in [11]. Using so-called Bridgestone model for generated muscle force, a dynamic torque model for model-based torque controller was derived in [12]. Similar static force description was used for deriving a static and dynamic model of McKibben pneumatic artificial muscle in [13]. In addition to using previously derived models, a finite element analysis method was applied to modelling of a pneumatic artificial muscle in [14]. All the mentioned works used constructionally simple McKibben muscles consisting of separated rubber tube enclosed by fibrous braiding. This type of pneumatic artificial muscles suffered from more pronounced nonlinear effects due to the friction between the rubber tube and braiding as well as between the fibres themselves. Moreover, it was also plagued by relatively high failure rate. Modifications to the basic pneumatic artificial muscle design by FESTO resulted in an actuator with improved characteristics and much better reliability. This type of pneumatic artificial muscle was used in [15] where a three-element phenomenological model was used for the representation of its characteristics as well as in [16] where improved geometric modelling of the shape of muscle was utilized. Also in [17, 18] a fundamental model of one-DOF pneumatic artificial muscle-based actuator with FESTO muscles was presented.

The motivation behind the work was to derive a model of one degree of freedom pneumatic muscle-based actuator for the purpose of control system design. As the derivation of a truth model for this system is quite complicated, it is necessary to consider control methods which are robust to modelling errors. Moreover the

system itself exhibits nonlinear and hysteretic behaviour what makes the suitability of linear controllers questionable. It is thus reasonable to assume the use of soft computing control methods (e.g. fuzzy or neural controller) [19, 20], the flexibility of which makes the adequate control of this system possible. On the other hand, grey modelling approach using the combination of first principle modelling and experimental determination of some parameters was selected over the pure black modelling since it has an advantage in preservation of model's universality and clear physical interpretation of modelled physical laws and used parameters.

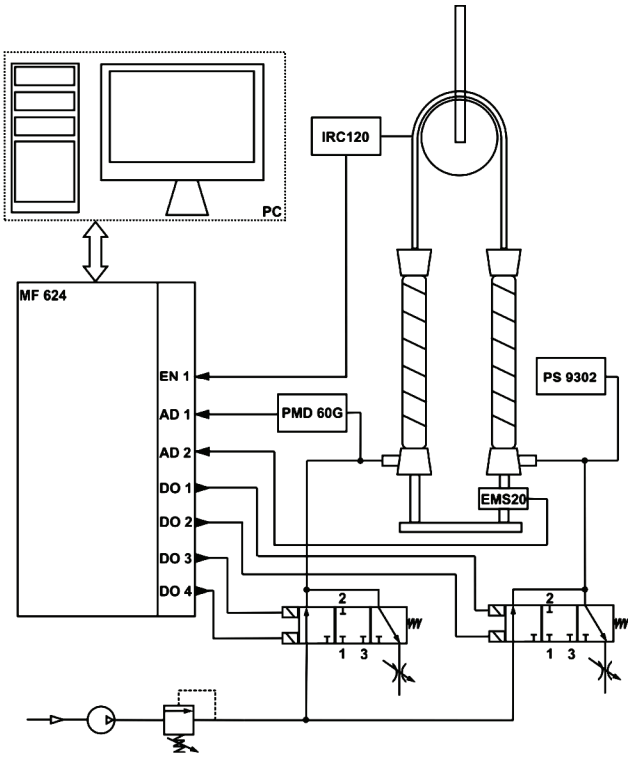

Figure 1 The schematic diagram of experimental setup

2 Experimental setup

In Fig. 1 the experimental setup used for measurement of relevant variables of actual actuator is depicted. The main part of the actuator is formed by two FESTO MAS-20 pneumatic artificial muscles with the length of 250 mm and fitted with the force compensator. The muscles are connected antagonistically through the chain gear and drive the shaft to which an arm with screwed weight is attached (not shown). The pressurized air was supplied by Fiac direct driven piston compressor. Two twin-solenoid 3/3 Matrix 821 valves with closed centre were used for controlling the pressurized air flow in a circuit. The valves were activated using the TTL-compatible logical signals fed from the digital outputs of I/O card (DO 1, 2, 3 and 4). Since the valve control voltage was 24 V, the low power TTL signal was only used for controlling the power transistors which provided the switching of high power signals from power supply. The PC used for data acquisition and processing was equipped with Intel Core 2 Quad 2.4 GHz processor and 4GB RAM and I/O interface was provided by Humusoft MF624 I/O card. Four sensors were used during the experiments: IRC120 encoder with 2500 pulses/ revolution, EMS20 force gauge with mV output and 0,5 % accuracy, Meret PMD-60G pressure converter with 0,5 % accuracy and Lutron PS-9302 pressure sensor with 0,5 % accuracy. The output of optical encoder proportional to the main (controlled) variable – arm angle – was fed into the encoder input of MF624 (EN 1).

The range of force gauge was 5 kN and its sensitivity was 1,5 mV/V, giving 15 mV output at 5000 N with 10 V supply voltage. The output signal had to be amplified using op-amp based differential amplifier and then fed into one of the analog inputs of MF624 (AD 2). The range of PMD-60G pressure converter was 600 kPa and its 0-10 V output signal could be fed directly into one of the card's analog inputs (AD 1). Lutron pressure sensor was used only for measuring the pressure in one of the muscles without feeding the output signal into the PC. All the work including the simulation, data acquisition and processing was carried in Matlab/Simulink environment. The sampling period was set to 0,0001 seconds.

3 Modelling

In order to obtain an analytical model of one-DOF pneumatic artificial muscle-based actuator, one has to derive a model of single muscle. A muscle model derivation is usually divided into two main parts, mechanical and pneumatic.

3.1 Mechanical part

Several fundamental models for pneumatic artificial muscles have been proposed up to this date and the model used here based on the modified Hill's muscle model [15] with variable damper [16]. This model assumes the parallel connection of a contractile element, variable damper and a spring, which can be seen in Fig. 2 for an antagonistic connection of two muscles.

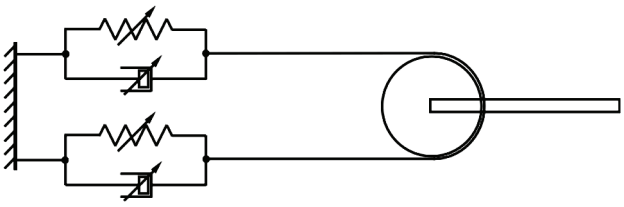

Figure 2 The representation of antagonistic connection of two muscles using the modified Hill's muscle model

The mechanical part can be described by the following nonlinear differential equation based (with further rearrangement of variables) on the Newton's second law:

$$m\ddot{y} + F_{\mathrm{S}}(k, P_{\mathrm{m}}) + F_{\mathrm{D}}(\dot{k}, P_{\mathrm{m}}) = F_{\mathrm{E}}, \tag{1}$$

$$\ddot{y} = \frac{1}{m}\left[F_{\mathrm{E}} - F_{\mathrm{S}}(k, P_{\mathrm{m}}) - F_{\mathrm{D}}(\dot{k}, P_{\mathrm{m}})\right], \tag{2}$$

where m – moving mass (kg), y – muscle displacement (m), $F_{\mathrm{S}}(k, P_{\mathrm{m}})$ – nonlinear term representing a variable

spring force (N), $F_D(\dot{k}, P_m)$ – nonlinear term representing a variable damper force (N), F_E – external force (N), k – muscle contraction (defined as $k = k_0 + y/l_0$ where k_0 is initial contraction and l_0 is initial muscle length) (–) and P_m – absolute muscle pressure (Pa).

Pneumatic artificial muscle behaves as a nonlinear spring, the stiffness of which can be controlled by the muscle pressure. The muscle static force (i.e. spring force) is thus the function of two variables, muscle contraction and muscle pressure. FESTO offers these characteristics as a part of product specifications and they are shown in Fig. 3 (for MAS-20). In order to model the depicted relationship, a fifth-order polynomial for two variables was used. This polynomial contained 21 coefficients and its form was as follows:

$$\begin{aligned} F_{CE} = {} & a_{00} + a_{10}k + a_{01}P_m + a_{20}k^2 + a_{11}kP_m + a_{02}P_m^2 + a_{30}k^3 + a_{21}k^2P_m + \\ & a_{12}kP_m^2 + a_{03}P_m^3 + a_{40}k^4 + a_{31}k^3P_m + a_{22}k^2P_m^2 + a_{13}kP_m^3 + a_{04}P_m^4 + \\ & a_{50}k^5 + a_{41}k^4P_m + a_{32}k^3P_m^2 + a_{23}k^2P_m^3 + a_{14}kP_m^4 + a_{05}P_m^5. \end{aligned} \quad (3)$$

The coefficient values were determined using Surface Fitting toolbox in MATLAB. The fit results are shown in Tab. 1 and approximated surface is shown in Fig. 4.

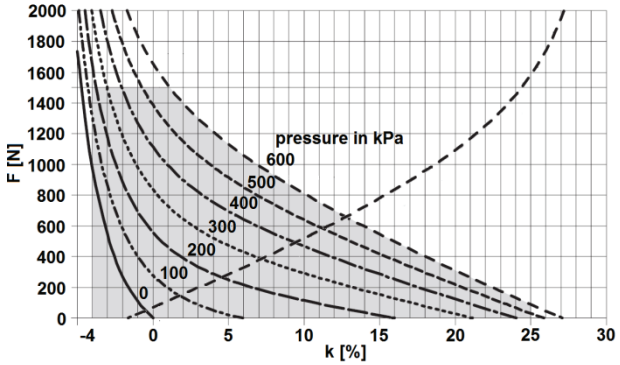

Figure 3 The relationship between the static muscle force and contraction for various muscle pressures (according to [19])

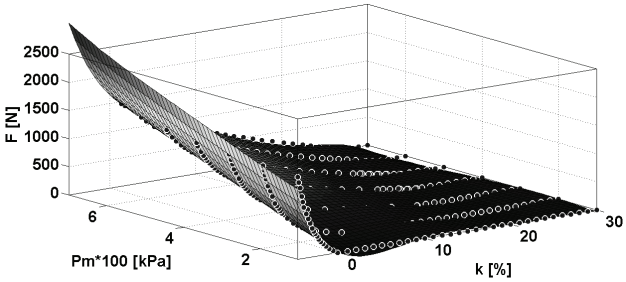

Figure 4 Force-contraction-pressure relationships approximated by the fifth-order polynomial

Table 1 Fit results for the fifth-order polynomial approximation

SSE	R-square	ad. R-square	RMSE
$5{,}1884\times10^5$	0,9918	0,9912	44,4159

The sum-squared error (SSE) in resulting fit is high due to the fact that zero force at higher values of contraction wasn't approximated very well (this is evident from Fig. 4). This fact, however, did not cause problems as the output of static force approximator was limited in simulation model to the range <0,1200>.

Actually, static characteristics for two muscles (connected antagonistically) are shown in Fig. 3. Due to the intended application area (industry), it was desirable to achieve as high stiffness as possible and thus only one muscle was active in one half of the arm movement range while the other one remained at the initial (high) pressure. The following equation for a joint stiffness derived in [22] shows that the stiffness is proportional to the sum of pressures in muscles:

$$K = \kappa_1(\theta)p_{10} + \kappa_2(\theta)p_{20} + \kappa_{atm}(\theta)p_{atm}, \quad (4)$$

where K – joint stiffness (N·m/rad), κ – muscle stiffness (N/m), p – relative muscle pressure (Pa), θ – arm angle (rad). For the given arm angle and one muscle pressure constant and high, the joint stiffness is higher than it would have been with symmetric filling/discharging. The intersections of the curves for various pressures in the first muscle correspond to the force equilibrium and steady-state arm angle.

The third term on the left side of (1) represents a damper force, which depends on (as usual) the muscle velocity but also on the muscle pressure [16]. The damper force term is nonlinear due to the multiplication of two functions. It can be written in the following form:

$$F_D(\dot{k}, P_m) = -RP_m\dot{k} \quad (5)$$

where R – damping coefficient ($m^2 \cdot s$), P_m – absolute muscle pressure (Pa) and $\dot{k}$ – muscle velocity (1/s).

The last term in (1) is F_E, which represents an external force to which a muscle is subjected. If one muscle is utilized, it can be the gravitational force of a load applied to it. In case of two muscles in antagonistic connection, it is the force of the other muscle.

3.2 Pneumatic part

The pneumatic part of the model is divided into two parts, the model of volume flow rate through the valves and a differential equation for the muscle pressure. Valves used for controlling the flow of pressurized air through the pneumatic circuit were of simple on-off type, meaning that the volume flow rate at constant compressor pressure (filling mode) or atmospheric pressure (discharge mode) depended solely on the muscle pressure. There are a number of various valve flow rate models, the application of which depends (also) on the availability of valve parameters. In [23] the following model, which has become a standard according to norm ISO 6358, was given:

$$\dot{V}_a = \begin{cases} P_1 C \sqrt{\dfrac{T_0}{T_1}} \sqrt{1 - \left(\dfrac{\dfrac{P_2}{P_1} - b}{1 - b} \right)^2}, & \text{if } \dfrac{P_2}{P_1} > b \\ P_1 C \sqrt{\dfrac{T_0}{T_1}}, & \text{if } \dfrac{P_2}{P_1} \le b \end{cases} \quad (6)$$

where $\dot{V}_a$ – volume flow rate (m^3/s), P_1 – absolute upstream pressure (Pa), C – sonic conductance (m^3/(s·Pa)), T_0 – ambient air temperature at reference conditions (K), T_1 – upstream temperature (K), P_2 – absolute downstream pressure (Pa) and b – critical ratio. The valve manufacturer gives the following values for Matrix 821 valves: C = 2,6167×10^{-9} m^3/(s·Pa) and b = 0,433.

In Fig. 5 the volume flow rates modelled according to (6) and using the parameters given by Matrix are shown. For the given compressor pressure, the volume flow rate through the valve is constant until the ratio of muscle and compressor pressures is larger than the critical ratio.

The shape of volume flow rate curves is different for filling and discharge modes as in former case P_1 is the compressor pressure and P_2 is the muscle pressure while in latter P_1 is the muscle pressure and P_2 is the atmospheric pressure.

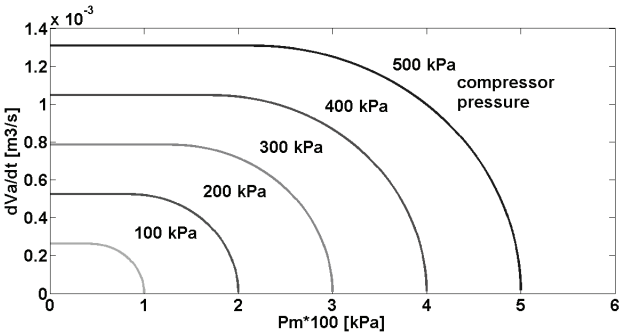

Figure 5 Modelled volume flow rate curves for Matrix 821 valves

The shape of volume flow rate curves is different for filling and discharge modes as in former case P_1 is the compressor pressure and P_2 is the muscle pressure while in latter P_1 is the muscle pressure and P_2 is the atmospheric pressure.

To complete the model of a pneumatic artificial muscle, the dependence of time rate of its pressure needs to be known. This equation can be derived from Boyle-Marriott's law for ideal gases, which can be written in the following form:

$$P_a V_a = P_m V_m, \tag{7}$$

where P_a – atmospheric pressure (Pa), V_a – volume of air in the muscle (m^3), P_m – muscle pressure (Pa) and V_m – muscle volume (m^3). For time derivative of muscle pressure we get:

$$\frac{\mathrm{d}}{\mathrm{d}t}\left(\frac{P_a V_a}{V_m}\right) = P_a\left(\frac{\dot{V}_a V_m - \dot{V}_m V_a}{V_m^2}\right) = P_a \frac{\dot{V}_a}{V_m} - P_m \frac{\dot{V}_m}{V_m}, \tag{8}$$

where $\dot{V}_a$ – time derivative of muscle air volume (volume flow rate through the valve (m^3/s) and $\dot{V}_m$ – time derivative of muscle volume (m^3/s). It follows from (8) that it is needed to know the muscle volume (and its time derivative) in order to be able to calculate the time derivative of muscle pressure. The muscle volume is a function of muscle contraction and it can be determined using certain geometric parameters of the muscle. In the simpler case it can be modelled as a cylinder, but due to the metal fittings at both ends of the muscle quite large deviations from this basic shape can be expected. A more accurate approach is to model it as a cylinder with two truncated hemispheres [16]. The resulting formula is rather complicated but it can be approximated well by using the third-order polynomial in this form:

$$V_m = ak^3 + bk^2 + ck + d, \tag{9}$$

where k – muscle contraction; a, b, c and d – polynomial coefficients. The coefficients were found out using Curve Fitting toolbox in MATLAB. The dependence of muscle volume on contraction is depicted in Fig. 6. The leftmost point on the curve in Fig. 6 corresponds to the rest volume of MAS-20 muscle with length of 250 mm which is approximately 0,079 dm^3.

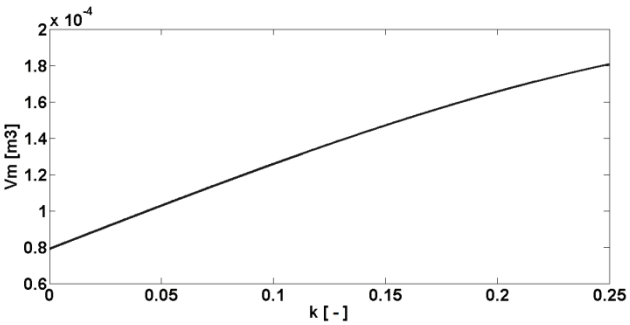

Figure 6 The dependence of muscle volume on its contraction

To conclude this part, the time derivative of muscle volume needs to be derived and it has the following form:

$$\dot{V}_m = 3ak^2\dot{k} + 2bk\dot{k} + c\dot{k}, \tag{10}$$

where $\dot{k}$ – muscle velocity, k – muscle contraction and a, b and c – polynomial coefficients (same as in (9)). By combining the equations (2), (3), (5), (6), (8), (9) and (10) the model of a single pneumatic muscle is derived.

3.3 Revolute joint

Kinematically, the examined system represents a one degree-of-freedom system with one revolute axis. The muscles provide the actuation of a steel shaft to which an arm with load mass is attached. From the dynamic point of view it can thus be modelled as a revolute joint plus actuator where the generalized variable would be the arm angle θ. It is important to note that the real plant's arm moved in a plane parallel to the ground (i.e. the rotational axis is parallel to the gravity force), meaning that the gravity effects can be neglected. If Lagrangian mechanics is used for deriving the joint dynamics, it can be written [24]:

$$\frac{\mathrm{d}}{\mathrm{d}t}\frac{\partial L}{\partial \dot{q}} - \frac{\partial L}{\partial q} = \tau, \tag{11}$$

where: $L = E_k - E_p$ – Lagrangian, q – generalized variable, τ – vector of generalized forces, E_k – kinetic energy and E_p – potential energy. For the examined case it is possible to write:

$$q = [\theta], \dot{q} = [\dot{\theta}], \tau = [T], E_k = \frac{1}{2} J\dot{\theta}^2, \quad (12)$$

where: θ – arm angle (rad), $\dot{\theta}$ - rotational speed (rad/s), T – torque (N·m), J – moment of inertia (kg·m^2). Of note is the fact that the potential energy ($E_p = mgh$) is not changing since the arm is moving in horizontal plane and thus can be chosen zero as only the differences in E_p are relevant [24]. If friction term (as well as gravity term due to the aforementioned reasons) is neglected, the joint dynamics is (J is considered constant):

$$\frac{\partial L}{\partial \dot{q}} = [J\dot{\theta}], \frac{d}{dt}\frac{\partial L}{\partial \dot{q}} = [J\ddot{\theta}] \quad (13)$$

$$J\ddot{\theta} = T - T_L, T = (F_1 - F_2)r \quad (14)$$

where T – torque provided by the muscles, T_L – load torque, F_1, F_2 – total muscle forces, r – gear wheel diameter.

4 Measurement and simulation results

The whole model was built and simulated in Matlab/Simulink environment. The time step was fixed to 0,0001 s and a continuous solver (ode8 Dormand Prince) was used. In order to validate the model, a number of real plant responses were obtained using the setup described in first paragraph. Due to the type of used valves (on-off), the responses were obtained using different times of valve opening from the same starting position. In this way, 15 responses corresponding to valve openings (T_0) from 0,1 s to 1,5 s were measured. The initial position (set-up position) corresponded to a zero arm angle with muscles pressurized to maximal operating pressures (approximately 550 kPa). For every valve opening period a set of five measurements was carried out and average values were considered. In Tab. 2 the main model parameters are shown.

Table 2 The main model parameters

Parameter	Value	Unit
Rest length, l_0	0,25	m
Moment of inertia, J	0,1143	kg·m^2
Damping coefficient, R	0,0007	m^{2}s
Initial contraction, k_0	10,8	%
Initial relative pressure, p_0	548	kPa
Initial force, F_0	695,8	N
Choking coefficient, η	0,43	-
Valve opening periods	0,1÷1,5	s

The results of measurement are summarized in Tab. 3. The values showed little variance after resetting the initial state during repeated measurements, making them suitable for comparison (standard deviations for the set of 15 average values of initial pressures are 0,06 % and 0,12 % respectively). Of note is a slight asymmetry in initial pressures of the muscles, which might be due to different positions of pressure sensors within the pneumatic circuit in relation to the muscles as well as the slight asymmetry in the initial arm position.

Table 3 The results of measurements for 15 valve opening periods

T_0 / s	p_{10} / kPa	p_{20} / kPa	p_{11} / kPa	p_{21} / kPa	k_{21} / %	θ / °
0,1	554,4	541,0	546,6	493,2	10,4	–2,34
0,2	554,8	542,4	539,6	450,4	9,6	–4,93
0,3	555,0	542,6	532,9	410,0	8,8	–7,45
0,4	554,8	542,2	525,8	373,2	8,6	–10,2
0,5	555,1	543,2	518,4	340,4	8,0	–13,0
0,6	555,3	543,6	512,1	308,8	7,2	–15,7
0,7	555,5	542,6	506,3	279,8	6,4	–18,4
0,8	555,4	542,8	500,7	252,8	6,0	–20,9
0,9	555,5	542,8	495,7	225,2	5,2	–23,6
1,0	555,5	542,6	491,7	201,0	4,8	–25,9
1,1	555,6	542,2	487,9	178,2	4,4	–27,9
1,2	555,5	542,2	484,8	156,6	4,0	–30,0
1,3	555,4	541,6	481,6	136,8	3,6	–31,9
1,4	555,3	542	478,2	117,6	2,8	–33,6
1,5	555,5	541,6	476,6	101,2	2,4	–35,2

The values given in Tab. 3 represent the steady-state values for significant variables: p_{10} – initial relative pressure of the first muscle (on the right side) (kPa), p_{20} – initial relative pressure of the second muscle (on the left side) (kPa), p_{11} – final relative pressure of the first muscle (kPa), p_{21} – final relative pressure of the second muscle (kPa), k_{21} – final value of the contraction of the second muscle (%), θ – steady-state arm angle (°).

The model was tested for the same set of valve opening periods with the initial pressure set to 548 kPa in both muscles. The steady-state values of relevant variables are shown in Tab. 4. In Fig. 7 the relative errors for model-predicted steady-state values of relevant variables are depicted.

Table 4 The model-predicted steady-state values

T_0 / s	p_0 / kPa	p_{11} / kPa	p_{21} / kPa	k_{21} / %	θ / °
0,1	548	538,6	501,6	10,4	–2,24
0,2	548	529,1	458,2	9,9	–4,6
0,3	548	519,7	417,7	9,4	–7,1
0,4	548	510,2	379,8	8,9	–9,59
0,5	548	500,8	344,4	8,4	–12,3
0,6	548	491,6	311,3	7,9	–15,0
0,7	548	482,4	280,3	7,3	–17,8
0,8	548	473,4	251,3	6,8	–20,6
0,9	548	464,7	224,1	6,2	–23,5
1,0	548	456,2	198,5	5,6	–26,4
1,1	548	448,2	174,3	5,0	–29,3
1,2	548	440,3	151,7	4,5	–32,3
1,3	548	433,5	129,9	3,9	–35,0
1,4	548	426,7	109,6	3,4	–37,9
1,5	548	421,4	89,8	2,9	–40,0

The relationship between δ_{p1} (relative error for p_1 prediction) and T_0 (valve opening period) is almost linear

implying the gradual error accumulation with the valve opening period. This might be due to small changes in the pressure compared to its initial value causing the corresponding muscle to stay mostly in linear part of its static characteristics. Conversely, δ_{p2} (relative error for p_2 prediction) shows greater variability and nonlinear character possibly caused by the corresponding muscle reaching the nonlinear part of its characteristics. Larger errors can be seen for arm angle and contraction prediction, which might be associated with the constancy of K_S parameter. The results of experiments with the model confirmed the dependence of K_S parameter on muscle pressure and the determination of this relationship is subject to further research. Moreover, it is also necessary to take into account the approximation error of (3).

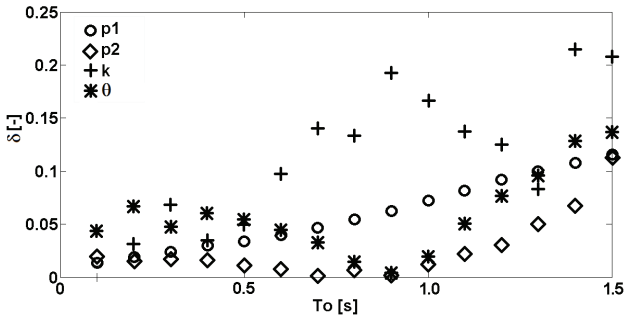

Figure 7 The relative errors for model-predicted variables

The dynamic validation of the model was carried out using the responses obtained from the sensors described in the first paragraph. The time period of measurements (as well as simulations) was set to $T = 2$ s. In Fig. 8 the dynamic position response to $T_0 = 0{,}1$ s is depicted. There is a small error in steady-state value prediction (Tab. 4) and the response is faster compared to the real plant. The relative damping of the response is slightly higher for model (15,4 % amplitude reduction for actuator and 13,6 % for model).

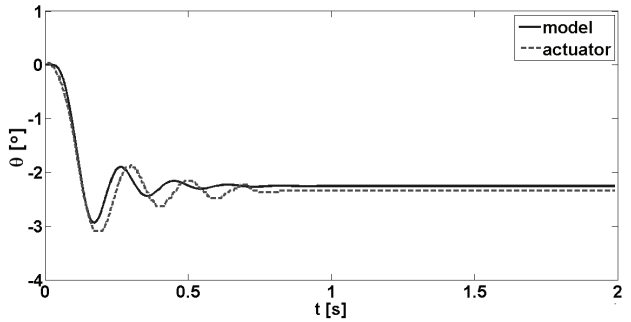

Figure 8 The predicted and measured dynamic responses for position ($T_0 = 0{,}1$ s)

In Fig. 9 the comparison of dynamic position responses to $T_0 = 0{,}3$ s is depicted. In this case, the relative error for position prediction increased to 4.9% (from 4,8 % for $T_0 = 0{,}1$ s) and the difference between the predicted and measured relative damping was 1,8 % (1,5 % amplitude reduction for actuator and 3,3 % for model). In accordance with the variable damper equation in (5), there is a change in damping with the changing muscle pressure. The difference between the amplitude reductions for $T_0 = 0{,}1$ s and $T_0 = 0{,}3$ s is 13,9 % for actuator and 10,3 % for model.

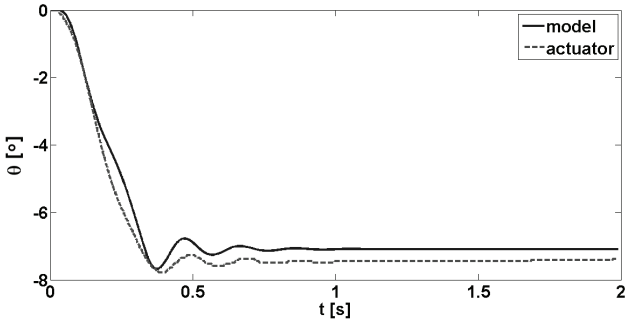

Figure 9 The predicted and measured dynamic responses for position ($T_0 = 0{,}3$ s)

In Figs. 10, 11 and 12, the responses to $T_0 = 0{,}5$ s, $T_0 = 0{,}7$ s and $T_0 = 0{,}9$ s respectively are shown. The relative errors for predicted position decrease gradually until certain point (6 %, 3 % and reaching minimum at 0,9 s 0,5 %). It can be seen that the predicted absolute and relative damping are both lower compared to the real actuator. It can be observed that the predicted damping was higher than the damping of real system for small arm angles and lower for larger arm angles implying certain inaccuracy in variable damper equation. At the current stage, these differences were not considered significant. The variation of predicted position error might be related to the asymmetric mechanic configuration of the actuator (the distance of muscles from the base was not equal) since the steady-state arm angle can be determined as $(l_1 - l_2)/r$ (it is also evident that there is a relationship between the predicted contraction error and the predicted position error – Fig. 7).

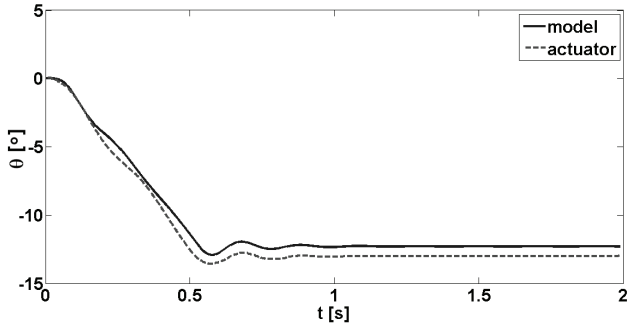

Figure 10 The predicted and measured dynamic responses for position ($T_0 = 0{,}5$ s)

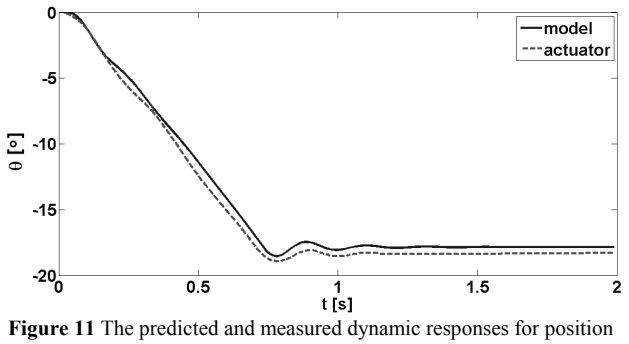

Figure 11 The predicted and measured dynamic responses for position ($T_0 = 0{,}7$ s)

In Fig. 13 the dynamic force responses of the real actuator to five valve opening periods are shown. It has to be noted that the responses are not completely steady

even after the disappearance of the oscillatory part of response, which is due to the high sensitivity of the force gauge and possible small leakage within the pneumatic circuit.

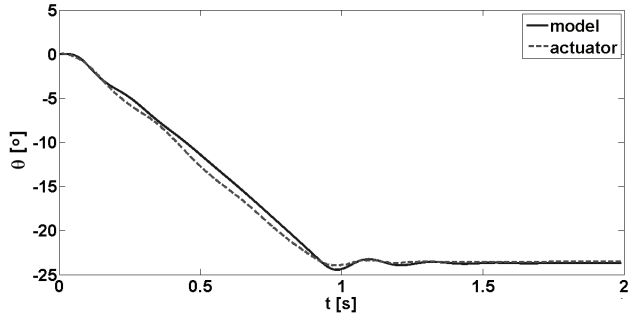

Figure 12 The predicted and measured dynamic responses for position (T_0 = 0,9 s)

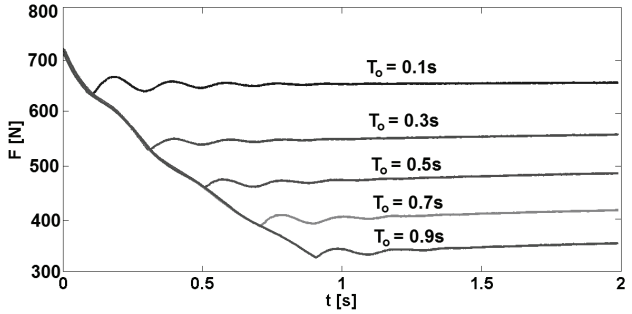

Figure 13 The measured dynamic responses for muscle force (five valve opening periods)

In Fig.14 the simulated responses to the same valve opening periods are shown.

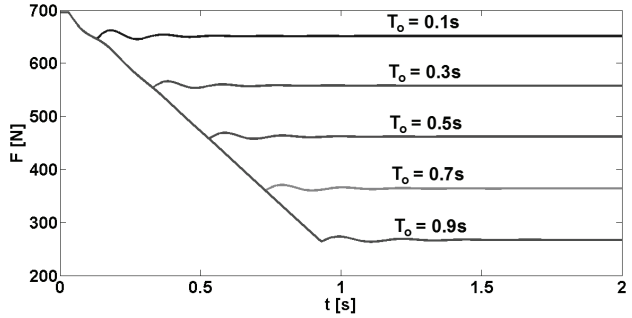

Figure 14 The simulated dynamic responses for muscle force (five valve opening periods)

It is clearly evident that the predicted force damping is higher compared to the real actuator. This difference probably arises from the simplified descriptions of the mechanical part of actuator.

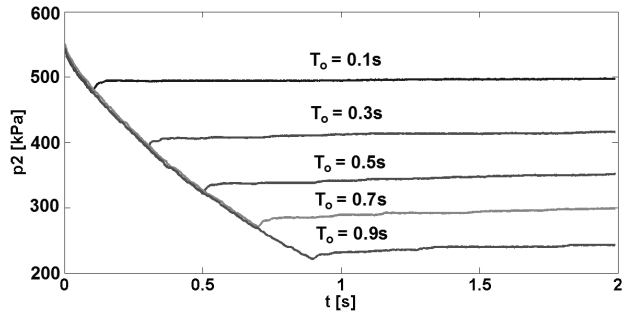

Figure 15 The measured dynamic responses for muscle pressure (five valve opening periods)

In Figs. 15 and 16 the measured and simulated muscles pressure responses to five valve opening periods are shown. Similarly to Fig. 13, the responses are not completely steady due to the sensitivity of bridge-resistance based pressure sensor. The steady-state values for both measurement and simulation can be found in Tabs. 3 and 4. It can be observed that the steady-state values as well as dynamic pressure responses for muscle pressure are in good correspondence.

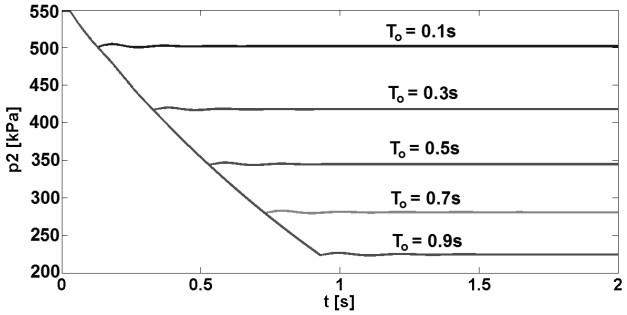

Figure 16 The simulated dynamic responses for muscle pressure (five valve opening periods)

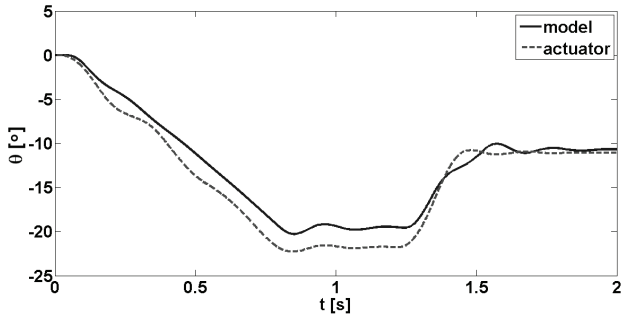

Figure 17 The predicted and measured responses to different valve opening periods for deflation and inflation modes (T_{od} = 0,76 s and T_{oi} = 0,28 s)

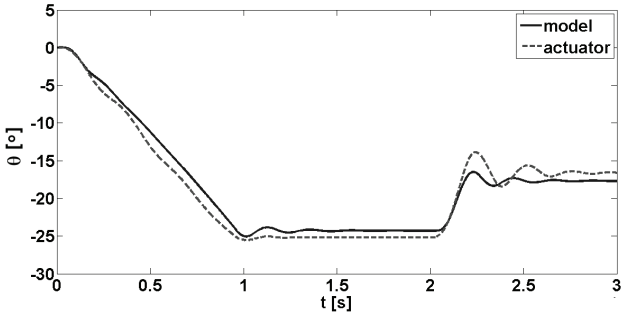

Figure 18 The predicted and measured responses to different valve opening periods for deflation and inflation modes (T_{od} = 0,92 s and T_{oi} = 0,16 s)

In Figs. 17 and 18 the predicted and measured responses to two different valve opening periods for filling and discharge modes are shown. In Fig. 17 the larger error for steady-state value in discharge mode can be seen which is in accordance with the modelling errors shown in Fig. 7. The error is, however, a bit larger in this case as the measured value did not fit between the values obtained during the first measurement (it should have been somewhere between (–18,4° and –20,9°). This can be ascribed to possible hysteresis effects and different initial conditions for the measurements. The filling mode steady-state value was predicted quite with the response being slightly slower compared to the real actuator. In

Fig. 18 the steady-state error for discharge mode is lower compared to the previous case (again in accordance with the values shown in Fig. 7). Of note are the differences in damping for filling and discharge modes. As was mentioned above, the equation (5) needs to be modified further in order to better describe the relationship between the damper force and muscle pressure (the muscle pressure spikes distinctive for the fast pressure changes are not so articulated which might be the cause of differences in predicted and measured damping).

5 Conclusion

The aim of this work was to build a model of one degree-of-freedom pneumatic artificial muscle-based actuator intended for applications in industry (Fig. 19).

This model was intended as a plant model capturing its dynamics that could be used for the control system design using simulation. The main idea behind the research was the design of control system for low-cost PAM-based system (hence the usage of on/off valves instead of proportional ones) using sophisticated nonlinear control techniques capable of handling the system's nonlinear and hysteretic properties.

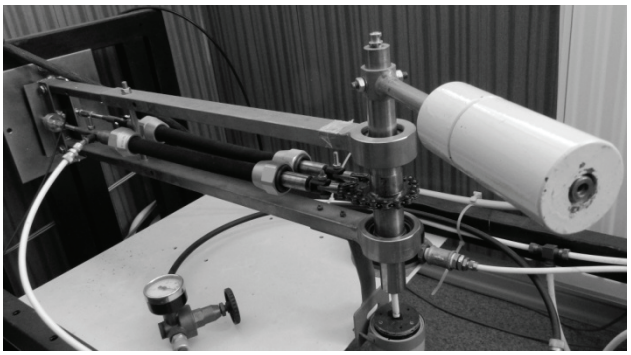

Figure 19 The PAM-based actuator photo

The selected method was to construct an analytical model using grey-box modelling (i.e. modelling using the combination of first principle modelling and experimental parameterization of the model). There is a definite advantage in using this method compared to a pure black-box modelling (e.g. using neuro/fuzzy modelling techniques) in obtaining a model with clear physical interpretation (concerning the modelled physical laws as well as the model parameters) what implies its universality (useful for modelling an actuator with muscles with different parameters for instance). On the other hand, the limitations of this method are also evident when the obtained results are examined. Accepted simplifications in modelling resulted in a model with higher modelling errors that would probably have been the case for neuro/fuzzy techniques. It is evident that this model could not be used as a truth model but it is acceptable as a model used for PAM-based industrial robot control design. There is a space for further refinement of the model in order to decrease the modelling errors so that the reliance on robustness of the control technique might be somewhat diminished.

Acknowledgements

The research work is supported by the Project of the Structural Funds of the EU, Operational Programme Research and Development, Measure 2.2 Transfer of knowledge and technology from research and development into practice. Title of the project: Research and development of nonconventional pneumatic artificial muscles-based actuators. ITMS code: 26220220103.

Podporujeme výskumné aktivity na Slovensku / Projekt je spolufinancovaný zo zdrojov ES.

6 References

[1] Orlovský, I.; Hatala, M.; Janák, M. Creation of simulation model of ceramic granulate production in spraying kiln. // Tehnicki vjesnik-Technical Gazette, 17, 4(2010), pp. 419-423.

[2] Tonkovic, Z. et al. Predicting natural gas consumption by neural networks. // Tehnicki vjesnik-Technical Gazette, 16, 3(2009), pp. 51-61.

[3] Sharma, V. et al. Multi response optimization of process parameters based on Taguchi-fuzzy model for coal cutting by water jet technology. // International Journal of Advanced Manufacturing Technology. DOI: 10.1007/s00170-011-3258-x

[4] Ivandić, Z.; Ergić, T.; Kljajin, M. Welding robots kinematic structures evaluation based on conceptual models using the potential method. // Tehnicki vjesnik-Technical Gazette, 16, 4(2009), pp. 35-45.

[5] Pilipović, A.; Raos, P.; Šercer, M. Experimental analysis of properties of materials for rapid prototyping. // International Journal of Advanced Manufacturing Technology, 40(2009), pp. 105-115.

[6] Lujić, R.; Šarić, T.; Heffer, G. Application of expert system for determination of the most beneficial suppliers in single production. // Tehnicki vjesnik-Technical Gazette, 16, 4(2009), pp. 81-6.

[7] Tozan, H.; Vayvay, O. Fuzzy Forecasting Applications on Supply Chains. // WSEAS Transactions on Systems, 7, 5(2008), pp. 600-609.

[8] Kovačić, Z.; Bogdan, S. Fuzzy Controller Design – Theory and Applications. // CRC Press – Taylor&Francis, Boca Raton, 2006.

[9] Chou, Ch.-P.; Hannaford, B. Measurement and Modeling of Pneumatic Artificial Muscles. // IEEE Transactions on Robotics and Automation, 12, 1(1996), pp. 90-102.

[10] Davis, S.; Caldwell, D. G. Braid Effects on Contractile Range and Friction Modeling in Pneumatic Muscle Actuators. // The International Journal of Robotics Research. 25, 4(2006), pp. 359-369.

[11] Davis, S.; Tsagarakis, N.; Canderle, J.; Caldwell, D.G. Enhanced Modelling and Performance in Braided Pneumatic Muscle Actuators. // The International Journal of Robotics Research, 22, 3-4(2003), pp. 213-227.

[12] Schroder, J.; Erol, D.; Kawamura, K.; Dillmann, R. Dynamic Pneumatic Actuator Model for a Model-Based Torque Controller. // International Symposium on Computational Intelligence in Robotics and Automation. Proceedings, Kobe, 2003, pp. 342-347.

[13] Colbrunn, R. W.; Nelson, G. M.; Quinn, R. D. Modeling of Braided Pneumatic Actuators for Robotic Control. //

International Conference on Intelligent Robots and Systems. Proceedings, Maui, 2001, pp. 1964-1970.
[14] Ramasamy, R. et al. An Application of Finite Element Modelling to Pneumatic Artificial Muscle. // American Journal of Applied Sciences, 11, 2(2005), pp. 1504-1508.
[15] Serres, J. L. Dynamic Characterization of a Pneumatic Muscle Actuator and Its Application to a Resistive Training Device. Dissertation thesis. Wright State University, 2008.
[16] Kerscher, T.; Albiez, J.; Zollner, J. M.; Dillmann, R. Evaluation of the Dynamic Model of Fluidic Muscles using Quick-release. // International Conference on Biomedical Robotics and Biomechatronics, Pisa, 2006, pp. 637-642
[17] Boržíková, J.; Piteľ, J.; Tóthová, M.; Šulc, B. Dynamic Simulation Model of PAM-based Antagonistic Actuator. // 12th International Carpathian Control Conference, Velké Karlovice, 2011.
[18] Neydorf, R.; Piteľ, J. An Approach to Universal Abstract Model of the Pneumatic Artificial Muscle. // Automation and Control in Theory and Practice ARTEP 2010. Proceedings, Stará Lesná, 2010, pp. 02-1-7.
[19] Castillo, O. et al. Comparative Study of Bio-inspired Algorithms Applied to the Optimization of Type-1 and Type-2 Fuzzy Controllers for an Autonomous Mobile Robot. // Information Sciences, 192(2012), pp. 19-38.
[20] Lopes, A. M.; Pires, E. J. S.; Barbosa, M. R. Design of a Parallel Robotic Manipulator Using Evolutionary Computing. // International Journal of Advanced Robotic Systems, 9(2012), pp. 1-13.
[21] FESTO – Fluidic Muscle DMSP/MAS, 2008. URL: http://www.festo.com/rep/en_corp/assets/pdf/info_501_en.pdf
[22] Verrelst, B. A Dynamic Walking Biped Actuated By Pleated Pneumatic Artificial Muscles: Basic Concepts and Control Issues. Dissertation thesis. Vrije Universiteit Brussel, 2005.
[23] Beater, P. Pneumatic Drives: System Design, Modelling and Control. Springer, New York, 2007
[24] Lewis, F. L.; Dawson, D. M.; Abdallah, Ch. T. Robot Manipulator Control: Theory and Practice. Marcel Dekker, New York, 2004

Authors' addresses

Hošovský Alexander
Department of Mathematics, Informatics and Cybernetics
Faculty of Manufacturing Technologies with seat in Prešov
Technical University of Košice
Bayerova 1, 08001 Prešov, Slovakia
alexander.hosovsky@tuke.sk

Havran Michal
Department of Mathematics, Informatics and Cybernetics
Faculty of Manufacturing Technologies with seat in Prešov
Technical University of Košice
Bayerova 1, 08001 Prešov, Slovakia
michal.havran@tuke.sk